Organometallic mechanism of action and inhibition of the 4Fe-4S isoprenoid biosynthesis protein GcpE (IspG)

Weixue Wang[a], Jikun Li[a], Ke Wang[b], Cancan Huang[a], Yong Zhang[c], and Eric Oldfield[a,b,1]

[a]Center for Biophysics and Computational Biology, University of Illinois at Urbana-Champaign, 607 South Mathews Avenue, Urbana, IL 61801; [b]Department of Chemistry, University of Illinois at Urbana-Champaign, 600 South Mathews Avenue, Urbana, IL 61801; and [c]Department of Chemistry and Biochemistry, University of Southern Mississippi, 118 College Drive #5043, Hattiesburg, MS 39406

Edited* by Christopher T. Walsh, Harvard Medical School, Boston, MA, and approved April 26, 2010 (received for review January 7, 2010)

We report the results of a series of chemical, EPR, ENDOR, and HYSCORE spectroscopic investigations of the mechanism of action (and inhibition) of GcpE, *E*-1-hydroxy-2-methyl-but-2-enyl-4-diphosphate (HMBPP) synthase, also known as IspG, an Fe_4S_4 cluster-containing protein. We find that the epoxide of HMBPP when reduced by GcpE generates the same transient EPR species as observed on addition of the substrate, 2-*C*-methyl-D-erythritol-2, 4-*cyclo*-diphosphate. ENDOR and HYSCORE spectra of these transient species (using ^2H, ^{13}C and ^{17}O labeled samples) indicate formation of an Fe-C-H containing organometallic intermediate, most likely a ferraoxetane. This is then rapidly reduced to a ferracyclopropane in which the HMBPP product forms an η^2-alkenyl π- (or π/σ) complex with the 4th Fe in the Fe_4S_4 cluster, and a similar "metallacycle" also forms between isopentenyl diphosphate (IPP) and GcpE. Based on this metallacycle concept, we show that an alkyne (propargyl) diphosphate is a good ($K_i \sim 300$ nM) GcpE inhibitor, and supported again by EPR and ENDOR results (a ^{13}C hyperfine coupling of ~7 MHz), as well as literature precedent, we propose that the alkyne forms another π/σ metallacycle, an η^2-alkynyl, or ferracyclopropene. Overall, the results are of broad general interest because they provide new mechanistic insights into GcpE catalysis and inhibition, with organometallic bond formation playing, in both cases, a key role.

4Fe-4S protein | GcpE (IspG) | metallacycle

Most pathogenic bacteria, plants, as well as malaria parasites (*Plasmodium* spp.), in contrast to humans, use the Rohmer, nonmevalonate or methyl erythritol phosphate pathway to produce isoprenoids (1, 2), so the development of inhibitors of this pathway is of interest in the context of drug (and herbicide) discovery. The structures of most of the enzymes in the pathway are now known from X-ray crystallography, but the structure of the penultimate enzyme, GcpE: *E*-1-hydroxy-2-methyl-but-2-enyl-4-diphosphate (**1**, HMBPP) synthase, EC 1.17.7.1, also known as IspG, has not yet been reported. Its mechanism of action is thus not well understood, and there is only one inhibitor (with an IC_{50} of ~1.6 mM) (3). GcpE enzymes catalyze the $2H^+/2e^-$ reduction of 2-*C*-methyl-D-erythritol-2,4-cyclo-diphosphate (**2**, MEcPP) to HMBPP:

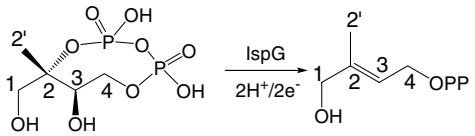

MEcPP (2) **HMBPP (1)**

All GcpEs contain three highly conserved Cys residues that are essential for catalysis and are thought to bind to an iron-sulfur cluster (4, 5). This cluster is, based on the results of Mössbauer (4) and EPR (5) spectroscopy, thought to have a 4Fe-4S composition. There have been several catalytic mechanisms proposed for GcpE. In one, Kollas et al. (6) proposed ring-opening of the cyclo-diphosphate to form a carbocation, followed by reduction to a radical, which then underwent reduction and dehydration to form the product, HMBPP (Fig. S1*A*). In a second mechanism, Seemann et al. (7) proposed a similar route, but with subsequent formation of a cation radical (Fig. S1*B*). In a third mechanism, Brandt et al. (8) proposed a cation → radical → anion mechanism (Fig. S1*C*). And in a fourth mechanism, Rohdich et al. (9) proposed that MEcPP underwent an OH^--assisted ring opening/ring closing to produce an oxirane **3**:

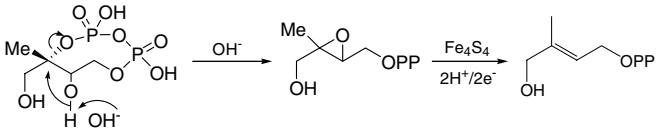

2 **3** **1**

that was then reduced to the alkene, **1**, via radical intermediates (Fig. S1*D*). The possible importance of an oxirane intermediate has also been described in recent work by Nyland et al. (10). There are, therefore, numerous mechanistic possibilities that have been proposed, and to try to clarify the GcpE mechanism, we report here the result of a series of spectroscopic observations on the structure of the intermediate reported by Adedeji et al. (5) that forms on addition of **2** to GcpE. This leads to a new GcpE mechanism as well as the discovery of a potent GcpE inhibitor.

Results and Discussion

EPR, ENDOR, and HYSCORE: Clues for Catalysis. We show in Fig. 1*A* the 9 GHz EPR spectrum of reduced IspG and in Fig. 1*B* the spectrum of the transient species that we shall call "X," formed in the presence of MEcPP. This spectrum could, in principle, arise from bound MEcPP, from a bound epoxide, from bound HMBPP, or from another reactive intermediate. To help distinguish between these possibilities, we prepared HMBPP-epoxide (a mixture of the 2R,3R and 2S,3S epoxides, formed by treating the bromohydrin of HMBPP with NH_3) and investigated its effect on the GcpE EPR spectrum. Remarkably, we find that the same EPR intermediate (X) as that formed on addition of MEcPP (Fig. 1*B*) forms on addition of HMBPP-epoxide to *Escherichia coli* GcpE (Fig. 1*C*), and the same results are obtained with *Thermus thermophilus* GcpE as well (Fig. S2). This argues against the bound MEcPP possibility for the reactive intermediate, X. In addition, the observation that the spectrum of MEcPP + GcpE (at long incubation

Author contributions: W.W. and E.O. designed research; W.W., J.L., K.W., C.H., and E.O. performed research; W.W., Y.Z., and E.O. analyzed data; J.L. and K.W. contributed new reagents/analytic tools; and E.O. wrote the paper.

The authors declare no conflict of interest.

*This Direct Submission article had a prearranged editor.

[1]To whom correspondence should be addressed. E-mail: eo@chad.scs.uiuc.edu.

This article contains supporting information online at www.pnas.org/lookup/suppl/doi:10.1073/pnas.1000264107/-/DCSupplemental.

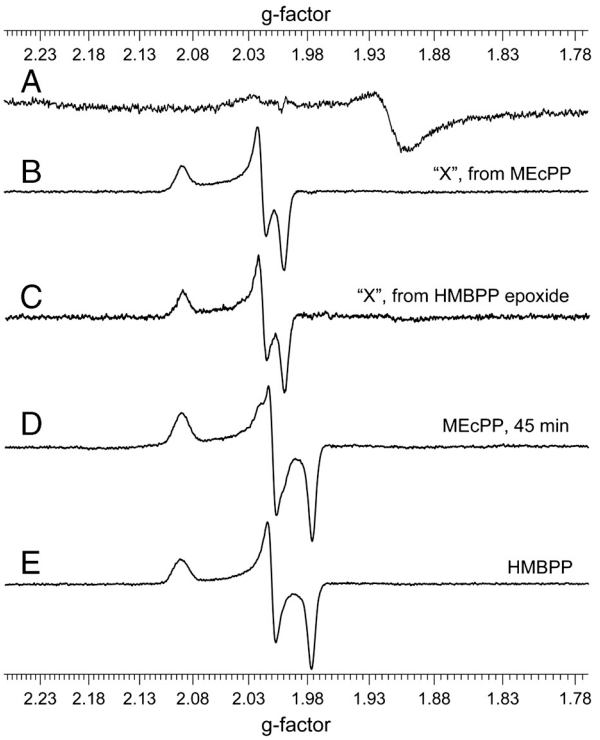

Fig. 1. X-band EPR spectra of GcpE ± reactants/products. (*A*) EPR of *E. coli* GcpE reduced with 20 equivalents $Na_2S_2O_4$. (*B*) EPR of *E. coli* GcpE + MEcPP, incubated for 1 min. (*C*) EPR of *E. coli* GcpE + HMBPP epoxide, incubated for 2 min. (*D*) EPR of *E. coli* GcpE + MEcPP, incubated for 45 min. (*E*) EPR of *E. coli* GcpE + HMBPP, incubated for 45 min. Frequency = 9.05 GHz, microwave power = 1 mW for *A*, 0.05 mW for *B–E*, temperature = 15 K.

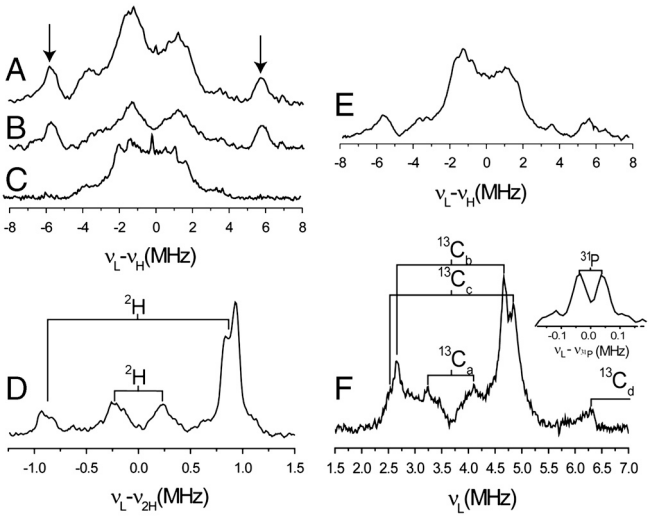

Fig. 2. X-band ENDOR of *T. thermophilus* GcpE + MEcPP/HMBPP-epoxide reaction intermediate X. (*A*) ^{1}H Davies ENDOR of GcpE + MEcPP. (*B*) ^{1}H Davies ENDOR of GcpE + MEcPP, in D_2O buffer. (*C*) ^{1}H Davies ENDOR of GcpE + [u-^{2}H]-MEcPP. (*D*) ^{2}H Mims ENDOR of GcpE + [u-^{2}H]-MEcPP, difference spectrum (^{2}H-labeled—unlabeled). (*E*) ^{1}H Davies ENDOR of GcpE + HMBPP epoxide. (*F*) ^{13}C Mims ENDOR of GcpE + [u-^{13}C]-MEcPP, difference spectrum (^{13}C-labeled—unlabeled). The inset is the unsubtracted ENDOR spectrum of the labeled sample showing the ^{31}P feature. Frequency = 9.66 GHz; spectra were collected at g_2 (B_0 = 342.2 mT) at 20 K. τ-averaging was used for collecting Mims ENDOR spectra as follows: *D* , 10 spectra at 8 ns steps with an initial τ = 248 ns; *F*, 12 spectra at 8 ns steps with an initial τ = 248 ns.

times) is identical to that found on HMBPP addition, with both *E. coli* (Fig. 1 *D* and *E*) and *T. thermophilus* GcpE (Fig. S3), rules out an HMBPP adduct as the origin of species X. The transient must, therefore, be either a bound epoxide, or another, as yet unknown, intermediate.

To explore this question in more detail, we next obtained the ^{1}H ENDOR spectra of X from unlabeled MEcPP. As shown in Fig. 2*A*, a ^{1}H ENDOR signal with a large hyperfine coupling ($A \sim 11.5$ MHz) is observed (the smaller central couplings are due to the Cys-beta protons). This ^{1}H ENDOR signal does not decrease on ^2H_2O exchange (four times, Fig. 2*B*) but is absent when [u-^{2}H]-MEcPP is used, Fig. 2*C*, so originates from the ligand. In this deuterated sample, we also find two sets of ^{2}H ENDOR signals in the low frequency region, Fig. 2*D*. The first has a large hyperfine coupling ($A \sim 1.8$ MHz) with a small quadrupole splitting and corresponds to the 11.5 MHz feature found in the ^{1}H ENDOR spectrum (Fig. 2*A*). The second set has a smaller coupling ($A \sim 0.5$ MHz) and arises from a weaker or long-range interaction with another deuteron in the ligand. We also find that the ^{1}H ENDOR spectrum of the intermediate X obtained by adding HMBPP epoxide (Fig. 2*E*) is very similar to that found with the MEcPP intermediate X (Fig. 2*A*).

The ^{13}C ENDOR spectrum of the reaction intermediate X obtained from [u-^{13}C]-MEcPP (Fig. 2*F*) shows several sets of peaks: One displays a small hyperfine coupling ($^{13}C_a$, $A \sim 0.84$ MHz); two sets have medium couplings ($^{13}C_b$, $A \sim 2.3$ MHz; $^{13}C_c$, $A \sim 2.3$ MHz); while one weak peak (at 6.3 MHz) could originate from the low frequency part of a much larger coupling ($^{13}C_d$, $A \sim 19$ MHz). The latter would have $|A/2| > \nu_L$ so would be centered at $|A/2|$, with two peaks separated by $2\nu_L$ (7.3 MHz at 342.2 mT), in which case the high frequency peak should appear at 13.6 MHz and would be obscured by the very strong ^{1}H peaks.

To help confirm these observations, we next obtained HYSCORE (hyperfine sublevel correlation) spectra (Fig. 3 *A–C*; expanded spectra are shown in Fig. S4). HYSCORE is a two dimensional form of pulsed EPR spectroscopy (11). In the (+/+) quadrant (on the right) of a HYSCORE spectrum, peaks due to weak interactions ($|A/2| < \nu_L$) are on the antidiagonal, while strong hyperfine interactions ($|A/2| > \nu_L$) are in the (+/−) quadrant (on the left), again on the antidiagonal. With unlabeled MEcPP, we see primarily the peak due to ^{14}N (most likely from protein backbone nitrogens (12), together with a natural abundance ^{13}C background (Fig. 3*A*), but with a ∼30% ^{13}C-enriched [2,3-^{13}C]-MEcPP (prepared biosynthetically from [2-^{13}C]-glucose and randomly ^{13}C-enriched only at C2,3) (13), there are now two additional sets of peaks: at (2.29, 5.14; 5.14, 2.29 MHz) in the (+/+) quadrant, and at (−4, 11; −11, 4 MHz) in the (+/−) quadrant, Fig. 3*B*. The former correspond to the peaks with medium couplings seen in ENDOR ($^{13}C_b$ or $^{13}C_c$ in Fig. 2*F*), while the latter correspond to the ^{13}C ENDOR peak with the large hyperfine coupling ($^{13}C_d$ in Fig. 2*F*). With a [u-^{13}C]-MEcPP labeled sample (having ∼100% ^{13}C), the signals are much stronger (Fig. 3*C*), and we now see that there is a third set of signals having a very small coupling (corresponding to $^{13}C_a$ seen in the ENDOR spectrum, Fig. 2*F*), plus, the cross-peaks with medium couplings in the (+/+) quadrant and the cross-peaks with the large coupling in the (+/−) quadrant are more intense. These results further narrow down the possible structures for the reactive intermediate X. Specifically, the GcpE-bound epoxide **4** is unlikely because nearly equal hyperfine couplings would be expected for C2 and C3, in sharp contrast to the large difference seen experimentally. But can we make other suggestions as to the nature of X, based on these spectroscopic results?

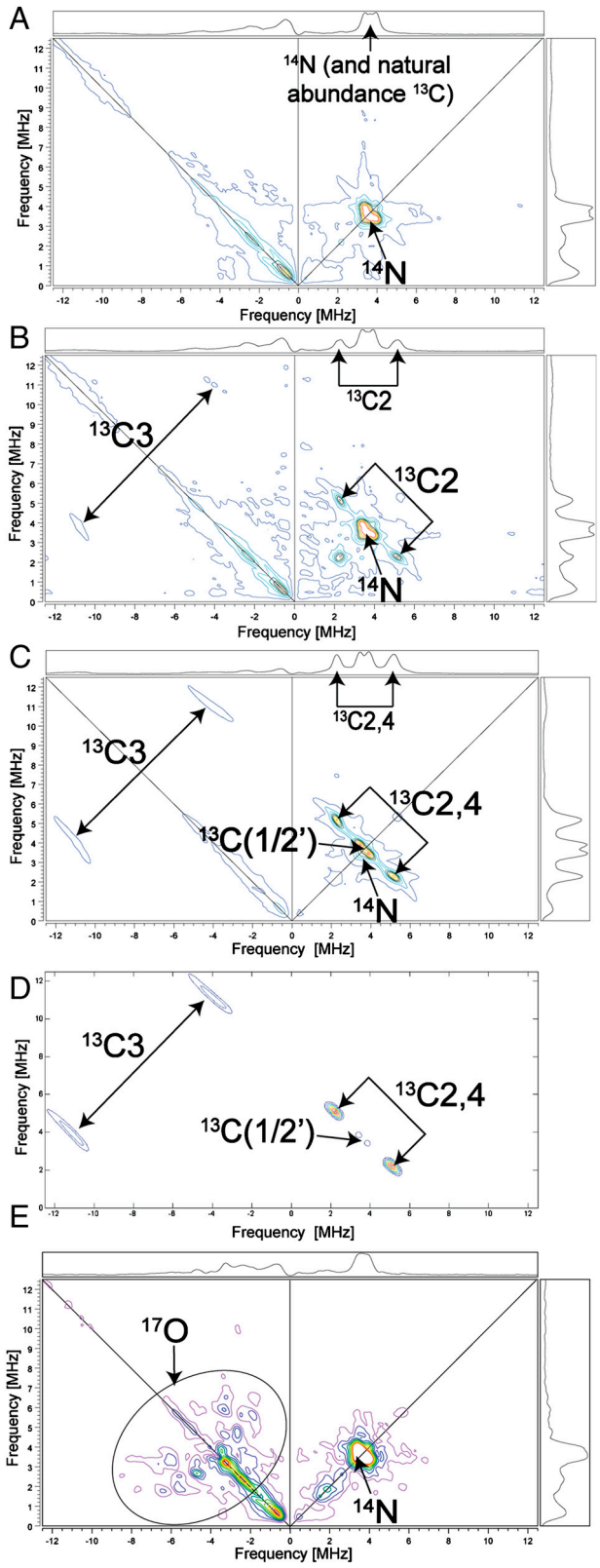

Fig. 3. HYSCORE spectra and simulation for *T. thermophilus* GcpE + MEcPP/HMBPP-epoxide reaction intermediate X. (*A*) GcpE + unlabeled MEcPP. (*B*) As *A* but with MEcPP enriched with (~30%) ^{13}C at C2 and/or C3. (*C*) As *A* but with [u-^{13}C]-HMBPP, 100% ^{13}C-labeled. The C1,2′ and 4 assignments are tentative. (*D*) Simulated ^{13}C spectrum with: C3 A_{ii} = [13,13,20] MHz; C2,4 A_{ii} = [2.3,2.3, 3.8] MHz; and C(1 or 2′) A_{ii} = [0.25,0.25,0.7] MHz. (*E*) GcpE + [2,3-^{17}O]-HMBPP epoxide. Frequency = 9.64 GHz, spectra were collected at ~g_2 (B_0 = 341.5 mT) at 18 K with τ = 136 ns. Expansions of the experimental spectra are shown in Fig. S4.

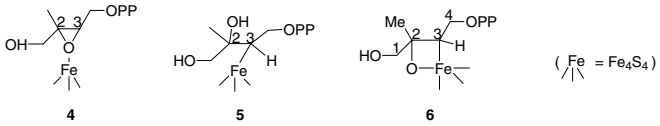

Organometallic Intermediates in GcpE Catalysis. The large (~16 MHz, Fig. 3*D*) ^{13}C hyperfine coupling observed in the [2,3-^{13}C]- and [u-^{13}C]-MEcPP samples suggested to us that X might contain an Fe-C bond in which the directly bonded carbon originates from C2 or C3 of MEcPP. This, when taken together with the 11.5 MHz ^{1}H ENDOR result, suggests that the strongly coupled ^{1}H is most likely directly bonded to the carbon that also has the large ^{13}C hyperfine coupling. The only proton in MEcPP that satisfies this constraint is H3, which then leads to two new candidates for X: the η^1-alkyl complex **5** and the ferraoxetane **6**. The difference between these two models is that in one case there is an Fe-O bond, while in the other, this bond is absent. To determine whether Fe-O bonding is present, we obtained the HYSCORE spectrum of X prepared from [2,3-^{17}O]-HMBPP epoxide (Fig. 3*E*). Features due to ^{17}O hyperfine/quadrupole interactions are clearly seen in the (+/−) quadrant, favoring the ferraoxetane **6** as the putative reaction intermediate X, although at present it is not certain whether it forms from **2** and **3** in a consecutive or parallel manner.

The possibility that the ferraoxetane **6** is a reaction intermediate is intriguing because many metallaoxatanes are known as stable species (14, 15), and in the case of Fe interacting with oxirane itself, the 1,2-ferraoxetane has been observed using matrix isolation (16). This species is more stable than is Fe+ oxirane (17), and on warming, the ferraoxetane undergoes a [2 + 2] dissociation to ethylene and FeO (16). The involvement of more complex metallaoxetanes in epoxide deoxygenation was proposed early on by Sharpless (18) (and would be essentially the opposite reaction to Sharpless epoxidation), and such species might be involved in oxirane deoxygenation by GcpE as well as by model Fe_4S_4 clusters (19). If the ferraoxetane does represent a reactive intermediate, a possible overall reaction mechanism is as shown at the top of the following Scheme, in which **6** is converted to the π/σ metallacycle **7** and product **1**:

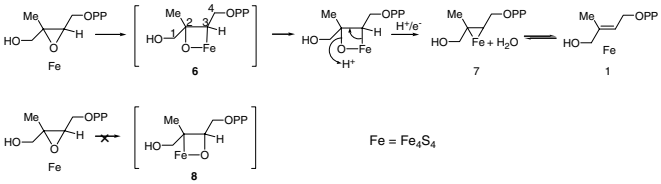

Initial formation of isomer **6** over the alternative species, **8**, seems likely, because as discussed earlier, the large ^{1}H hyperfine coupling is consistent with a 2-bond rather than a 3-bond interaction of the iron-sulfur cluster with H3. Ring formation might also proceed via radical intermediates, but the EPR and ENDOR results we do see provide no evidence for any stable, carbon-based radicals, which would have *g*-values at about the free electron *g*-value. But is there any evidence that the HMBPP metallacycle **7** actually forms? And if it does, can this help us find new inhibitors?

HMBPP (and IPP) Form Metallacycles with GcpE. We next consider the question as to whether the HMBPP product does in fact bind to the Fe_4S_4 cluster in GcpE. Because HMBPP is, chemically, just a substituted ethylene or allyl alcohol, and because ethylene and allyl alcohol are known to form π (or π/σ) η^2-alkenyl "metallacycle" complexes with a nitrogenase FeMo cofactor (which is thought to contain a Fe_3MoS_3X cubane-like structure) (20, 21), we

reasoned that HMBPP bound to GcpE might also form a π (or π/σ) complex with the unique fourth Fe in the Fe_4S_4 cluster. As noted above, we find that there are very large changes in the EPR spectra of GcpE on addition of HMBPP (or MEcPP, at ~45 min) (Fig. 1 *A*, *D*, and *E*), indicating major changes in the cluster's electronic structure. To test the metallacycle hypothesis further, we obtained the ENDOR spectrum of [u-^{13}C]-HMBPP bound to *T. thermophilus* GcpE, Fig. 4 *A* and *B*. As can be seen in Fig. 4*A*, there are ENDOR resonances due to ^{13}C hyperfine coupling (Fig. 4*A*, $A \sim 1.4$ MHz), together with a small ^{31}P coupling (Fig. 4*B*, $A \sim 0.3$ MHz), consistent with the idea that HMBPP is bound to GcpE, forming a π (or π/σ) η^2-alkenyl metallacycle, as illustrated schematically in Fig. 4*C*. This type of interaction also occurs with isopentenyl diphosphate (IPP), because as shown in Fig. 4*D*, a narrow line spectrum (with $g = 2.065$, 1.995 and 1.975) is obtained for GcpE (from *T. thermophilus*) in the presence of IPP, and ^{13}C and ^{31}P ENDOR signals are found on binding of [4-$^{13}C_1$]-IPP, Fig. 4 *E* and *F*. So, HMBPP and IPP, both of which contain alkene groups, interact with the reduced Fe_4S_4 cluster in GcpE, forming, we propose, η^2-alkenyl π (or π/σ) metallacycles, basically the same type of structure as seen with ethylene or allyl alcohol (the HMBPP "parent" molecules) bound to the nitrogenase FeMo cofactor. Notably, this type of π-complex formation is also found with reduced LytB (22), the last enzyme in the nonmevalonate pathway. And because there is no 1-OH group in IPP, alkoxide binding as in LytB (23) is not essential for interaction with the Fe_4S_4 cluster.

Discovery of Potent GcpE Inhibition Involving a Metallacycle (π or π/σ) Complex. The results described above, in which we find evidence for organometallic (π or π/σ) complexes, led to new ideas for GcpE inhibitors. In their work on alkyne reductions by model Fe_4S_4 clusters, Itoh et al. (24) discovered that diphenylacetylene was reduced to *cis*-stilbene. This is reminiscent of the reduction of acetylene to ethylene catalyzed by $[Fe_4S_4(SPh)_4]^{2-/3-}$/HOAc/Ac_2O reported by McMillan et al. (25), where it was suggested that the reaction involved formation of a π or π/σ complex in which acetylene binds to one of the Fe atoms, with species (resonance hybrids) such as **9a**, **9b** being formed. Direct evidence for π complex formation between an alkyne and an Fe_4S_4 cluster has been observed by Tanaka et al. (26), who found that the C ≡ C vibrational Raman frequency of acetylene decreased by ≈60 cm^{-1} when bound to $[Fe_4S_4(SPh)_4]^{3-}$ and was accompanied by the loss of one PhS^- ligand (as determined by UV-VIS spectroscopy).

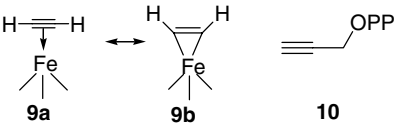

Taken together, this literature as well as our ENDOR results suggested to us that because alkenes and alkynes can bind to Fe_4S_4 clusters, species such as **10**, propargyl diphosphate, might be GcpE inhibitors, forming η^2-alkynyl complexes, just as they do with LytB (22).

The EPR spectrum of propargyl diphosphate **10** bound to *E. coli* GcpE exhibited a narrow line spectrum (Fig. 5*A*) clearly distinct from that observed in the absence of the ligand (Fig. 1*A*). A similar result was obtained for *T. thermophilus* GcpE + **10** (Fig. 5*B*). There is, therefore, a major change in the electronic structures of both clusters on binding this acetylenic compound, and the results of an ENDOR experiment using [u-$^{13}C_3$]-**10** (Fig. 5*C*) indicates a large ($A \sim 7$ MHz) ^{13}C hyperfine interaction. As with HMBPP and IPP binding, these results suggest formation of a π (or π/σ) complex, a ferracyclopropene. Notably, the ^{13}C hyperfine couplings in the alkyne are much larger than those found in any of the alkene complexes (~1–3.7 MHz) (20, 22), suggesting stronger binding with the alkyne. This could be due solely to the fact that alkynes are better donors/acceptors than are alkenes, but in this particular system it might also be due to the presence of "resonance" forms that could stabilize alkyne bonding—not dissimilar to the presence of resonance in, e.g., the cyclopropenyl cation [which like some metallacycles (27), is aromatic]. Consistent with the stronger binding affinity suggested by these spectroscopic results, we find that propargyl diphosphate (**10**) is a competitive GcpE inhibitor with an $IC_{50} \sim 750$ nM ($K_i \sim 330$ nM) (Fig. 5*D*) binding we propose as the π (or π/σ)

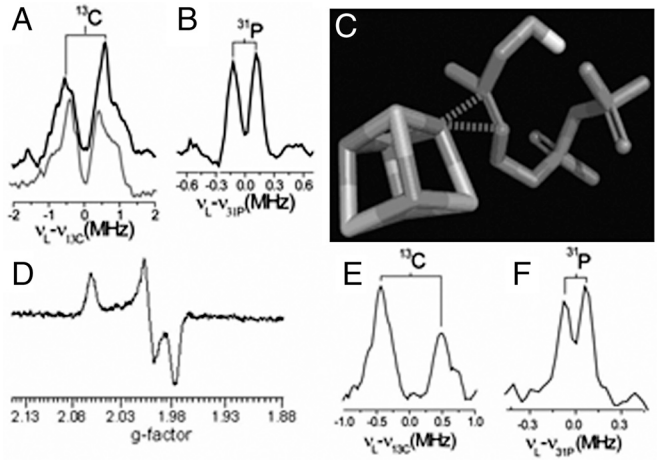

Fig. 4. X-band EPR and ENDOR spectra of GcpE (and IspH) + HMBPP/IPP. (*A*) ^{13}C ENDOR of GcpE + [u-^{13}C]-HMBPP, difference spectrum (^{13}C-labeled—unlabeled). The bottom inset is the *A. aeolicus* IspH E126A mutant + [u-^{13}C]-HMBPP (from ref. 22). (*B*) ^{31}P ENDOR of GcpE + [u-^{13}C]-HMBPP. (*C*) Schematic illustration of HMBPP bound to an Fe_4S_4 cluster illustrating metallacycle formation. (*D*) EPR of GcpE + IPP. (*E*) ^{13}C ENDOR of GcpE + [4-^{13}C]-IPP, difference spectrum (^{13}C-labeled–unlabeled). (*F*) ^{31}P ENDOR of GcpE + [4-^{13}C]-IPP. EPR frequency = 9.05 GHz; ENDOR frequency = 9.66 GHz; B_0 was selected as the field where the maximum EPR signal intensity was obtained: *A* and *B*, 347.9 mT; *E* and *F*, 344.4 mT. τ-averaging (64 spectra at 8 ns step with initial $\tau = 200$ ns) were used for collecting the Mims ENDOR spectra.

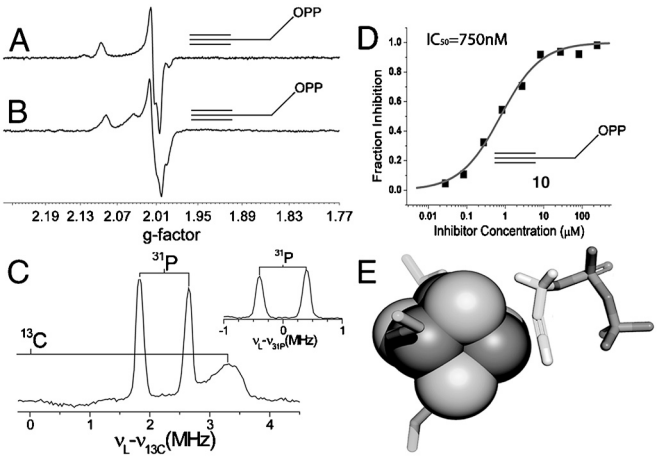

Fig. 5. Inhibition of GcpE by an alkynyl diphosphate **10** also involves metallacycle formation. (*A*) 9.05 GHz EPR of *E. coli* GcpE + 10 equivalents propargyl diphosphate **10** and 20 equivalents sodium dithionite. (*B*) 9.05 GHz EPR of *T. thermophilus* GcpE + 10 equivalents propargyl diphosphate **10** and 20 equivalents sodium dithionite. (*C*) ENDOR of *T. thermophilus* GcpE + [u-^{13}C] propargyl diphosphate **10**. The inset is the ENDOR spectrum of GcpE + unlabeled **10**, showing only the ^{31}P signals. Frequency = 9.66 GHz; Spectra were collected at 15 K at $B_0 = 342.4$ mT, where the maximum EPR signal intensity was obtained. τ-averaging (64 spectra at 8 ns steps with initial $\tau = 200$ ns) was used. (*D*) *E. coli* GcpE inhibition by propargyl diphosphate, $IC_{50} = 750$ nM ($K_i \sim 330$ nM). (*E*) Schematic illustration (based on LytB + **10** docking calculation) (22) of how propargyl diphosphate might bind to GcpE, forming an η^2-alkynyl complex.

complex (Fig. 5*E*) and is ~1,000× more potent than previously reported GcpE inhibitors (3).

Conclusions

The results we have described above are of interest for several reasons. First, we find that the EPR spectrum of the reactive intermediate X formed on MEcPP addition is the same as that found on HMBPP-epoxide addition, indicating that both MEcPP and HMBPP-epoxide form the same intermediate. Second, we propose a tentative structure for this intermediate: an Fe-C-H containing (organometallic) species, most likely a ferraoxetane, based on the results of ^{1}H, ^{2}H, ^{13}C, and ^{17}O ENDOR and HYSCORE experiments. Third, we propose that HMBPP, as well as IPP, form π (or π/σ) metallacycle complexes, ferracyclopropanes, based on the EPR and ENDOR results and precedent. Fourth, we find that an alkynyl diphosphate, propargyl diphosphate, is a good (IC_{50} = 750 nM) GcpE inhibitor lead that also forms a metallacycle (a π or π/σ, η^2-alkynyl) complex with the Fe_4S_4 cluster, based on the large hyperfine coupling seen in its ENDOR spectrum and on literature precedent for acetylene/Fe_4S_4 cluster interactions in model systems. These results lead to the idea that, in the future, it may be possible to develop related compounds as novel drugs targeting isoprenoid biosynthesis and that organometallic complex formation may play a role in reactions catalyzed by other Fe_4S_4-containing proteins containing "unique," fourth Fe atoms.

Methods

Pulsed ENDOR/HYSCORE spectra were obtained on a Bruker ElexSys E-580-10 FT-EPR X-band EPR spectrometer using a Bruker RF amplifier (150 W, 100 kHz–250 MHz, for pulsed ENDOR experiments) and an Oxford Instruments CF935 cryostat. Mims pulsed ENDOR used a three-pulse sequence ($\pi/2_{mw}$-τ-$\pi/2_{mw}$–T – $\pi/2_{mw}$-τ-echo; $\pi/2_{mw}$ = 16 ns, with π_{RF} applied during T). τ-averaging was used to reduce the blind spots that arise from the τ-dependent oscillations. Davies pulsed ENDOR used a three-pulse sequence (π_{mw} – T-$\pi/2_{mw}$ – τ – π_{mw}-τ-echo; $\pi/2_{mw}$ = 48 ns, with π_{RF} applied during T). HYSCORE used a four-pulse sequence ($\pi/2_{mw}$ – τ-$\pi/2_{mw}$ – t_1 – π_{mw} – t_2 – $\pi/2_{mw}$ – echo; $\pi/2_{mw}$ = 16 ns), 256 points for both t_1 and t_2, each at 20 ns steps. Time-domain data were baseline corrected using a third order polynomial, then Hamming windowed, followed by zero-filling and 2D-Fourier transformation. The HYSCORE spectrum was simulated using the EasySpin program package (28).

Additional details on protein purification and reconstitution, enzyme assays, EPR/ENDOR/HYSCORE sample preparation, and compound syntheses are reported in *SI Methods*.

ACKNOWLEDGMENTS. We are grateful to Pinghua Liu for providing his *E. coli* GcpE expression system and to H. Jomaa and J. Wiesner for providing their *T. thermophilus* GcpE expression systems. We thank Mark J. Nilges for helpful discussions and assistance with the ENDOR and pulsed EPR experiments, and Thomas B. Rauchfuss, John Hartwig, Wilfred van der Donk, Yonghui Zhang, Evert Duin, and Sergei Dikanov, for their helpful suggestions. This work was supported by the United States Public Health Service (National Institutes of Health Grant GM65307).

1. Rohmer M (2008) From molecular fossils of bacterial hopanoids to the formation of isoprene units: Discovery and elucidation of the methylerythritol phosphate pathway. *Lipids* 43:1095–1107.
2. Rohmer M, Grosdemange-Billiard C, Seemann M, Tritsch D (2004) Isoprenoid biosynthesis as a novel target for antibacterial and antiparasitic drugs. *Curr Opin Invest Drugs* 5:154–162.
3. Van Hoof S, et al. (2008) Synthesis of analogues of (*E*)-1-hydroxy-2-methylbut-2-enyl 4-diphosphate, an isoprenoid precursor and human gamma delta t cell activator. *J Org Chem* 73:1365–1370.
4. Seemann M, et al. (2005) Isoprenoid biosynthesis in chloroplasts via the methylerythritol phosphate pathway: The (*E*)-4-hydroxy-3-methylbut-2-enyl diphosphate synthase (GcpE) from *Arabidopsis thaliana* is a [4Fe-4S] protein. *J Biol Inorg Chem* 10:131–137.
5. Adedeji D, et al. (2007) Possible direct involvement of the active-site [4Fe-4S] cluster of the GcpE enzyme from *Thermus thermophilus* in the conversion of MEcPP. *FEBS Lett* 581:279–283.
6. Kollas AK, et al. (2002) Functional characterization of GcpE, an essential enzyme of the non-mevalonate pathway of isoprenoid biosynthesis. *FEBS Lett* 532:432–436.
7. Seemann M, et al. (2002) Isoprenoid biosynthesis through the methylerythritol phosphate pathway: The (*E*)-4-hydroxy-3-methylbut-2-enyl diphosphate synthase (GcpE) is a [4Fe-4S] protein. *Angew Chem Int Ed Engl* 41:4337–4339.
8. Brandt W, et al. (2004) A proposed mechanism for the reductive ring opening of the cyclodiphosphate MEcPP, a crucial transformation in the new DXP/MEP pathway to isoprenoids based on modeling studies and feeding experiments. *Chembiochem* 5:311–323.
9. Rohdich F, et al. (2003) The deoxyxylulose phosphate pathway of isoprenoid biosynthesis: Studies on the mechanisms of the reactions catalyzed by IspG and IspH protein. *Proc Natl Acad Sci USA* 100:1586–1591.
10. Nyland RL, II, Xiao Y, Liu P, Freel Meyers CL (2009) IspG converts an epoxide substrate analogue to (*E*)-4-hydroxy-3-methylbut-2-enyl diphosphate: Implications for IspG catalysis in isoprenoid biosynthesis. *J Am Chem Soc* 131:17734–17735.
11. Schweiger A, Jeschke G (2001) *Principles of pulse electron paramagnetic resonance* (Oxford Univ Press, Oxford).
12. Dikanov SA, Samoilova RI, Kappl R, Crofts AR, Huttermann J (2009) The reduced [2Fe-2S] clusters in *adrenodoxin* and *arthrospira platensis* ferredoxin share spin density with protein nitrogens, probed using 2D ESEEM. *Phys Chem Chem Phys* 11:6807–6819.
13. Eisenreich W, Bacher A, Arigoni D, Rohdich F (2004) Biosynthesis of isoprenoids via the non-mevalonate pathway. *Cell Mol Life Sci* 61:1401–1426.
14. Hashmi AS, Hutchings GJ (2006) Gold catalysis. *Angew Chem Int Ed Engl* 45:7896–7936.
15. Calhorda MJ, et al. (1993) Rhodaoxetane—Synthesis, structure, and theoretical evaluation. *Organometallics* 12:3316–3325.
16. Kafafi ZH, Hauge RH, Billups WE, Margrave JL (1987) Infrared-spectroscopy and photochemistry of iron ethylene-oxide in cryogenic matrices—The FTIR spectrum of vinyliron hydroxide. *J Am Chem Soc* 109:4775–4780.
17. Backvall JE, Bokman F, Blomberg MRA (1992) Metallaoxetanes as possible intermediates in metal-promoted deoxygenation of epoxides and epoxidation of olefins. *J Am Chem Soc* 114:534–538.
18. Sharpless KB, Teranishi AY, Backvall JE (1977) Chromyl chloride oxidations of olefins—Possible role of organometallic intermediates in oxidations of olefins by oxo transition-metal species. *J Am Chem Soc* 99:3120–3128.
19. Itoh T, Nagano T, Sato M, Hirobe M (1989) Deoxygenation of oxiran compounds to olefins by $[Fe_4S_4(SC_6H_5)_4]^{2-}$ in the presence of $NaBH_4$. *Tetrahedron Lett* 30:6387–6388.
20. Lee HI, et al. (2004) An organometallic intermediate during alkyne reduction by nitrogenase. *J Am Chem Soc* 126:9563–9569.
21. Pelmenschikov V, Case DA, Noodleman L (2008) Ligand-bound S = 1/2 FeMo-cofactor of nitrogenase: Hyperfine interaction analysis and implication for the central ligand X identity. *Inorg Chem* 47:6162–6172.
22. Wang W, et al. (2010) Bioorganometallic mechanism of action, and inhibition, of IspH. *Proc Natl Acad Sci USA* 107:4522–4527.
23. Gräwert T, et al. (2010) Probing the reaction mechanism of IspH protein by X-ray structure analysis. *Proc Natl Acad Sci USA* 107:1077–1081.
24. Itoh T, Nagano T, Hirobe M (1980) $[Fe_4S_4(SR)_4]^{2-}$ catalytic reduction of diphenylacetylene to *cis*-stilbene in the presence of $NaBH_4$. *Tetrahedron Lett* 21:1343–1346.
25. McMillan RS, Renaud J, Reynolds JG, Holm RH (1979) Biologically related iron-sulfur clusters as reaction centers. Reduction of acetylene to ethylene in systems based on $[Fe_4S_4(SR)_4]^{3-}$. *J Inorg Biochem* 11:213–227.
26. Tanaka K, Nakamoto M, Tsunomori M, Tanaka T (1987) Raman-spectra of the adducts of reduced species of $[Fe_4S_4(SPh)_4]^{2-}$ and $[Mo_2Fe_6S_8(SPh)_9]^{3-}$ with acetylene. *Chem Lett* 613–616.
27. Periyasamy G, Burton NA, Hillier IH, Thomas JM (2008) Electron delocalization in the metallabenzenes: A computational analysis of ring currents. *J Phys Chem A* 112:5960–5972.
28. Stoll S, Schweiger A (2006) EasySpin, a comprehensive software package for spectral simulation and analysis in EPR. *J Magn Reson* 178:42–55.